IOP Conference Series: Materials Science and Engineering

PAPER • OPEN ACCESS

Effect of UV-activated TiO_2 Nanoparticles on the Properties and Performance of PAni-TiO_2 Nanocomposite Films for Solar Cell Applications

To cite this article: F. M. El-Hossary *et al* 2020 *IOP Conf. Ser.: Mater. Sci. Eng.* **956** 012015

IOP Conf. Series: Materials Science and Engineering **956** (2020) 012015 doi:10.1088/1757-899X/956/1/012015

Effect of UV-activated TiO_2 Nanoparticles on the Properties and Performance of PAni-TiO_2 Nanocomposite Films for Solar Cell Applications

F. M. El-Hossary [1], A. Ghitas [2], A. M. Abd El-Rahman [3, 1], A. A. Ebnalwaled [4,5], M. Abdelhamid Shahat [2,*], M. H. Fawey [1]

[1] Physics Department, Faculty of Science, Sohag University, 82524 Sohag, Egypt.
[2] Photovoltaic Unit, Solar and Space Research Department, National Research Institute of Astronomy and Geophysics (NRIAG), 11421 Helwan, Cairo, Egypt.
[3] King AbdulAziz University, Jeddah, KSA.
[4] Electronics & Nano Devices Lab, Physics Department, Faculty of Science, South Valley University, 83523 Qena, Egypt.
[5] Egypt Nanotechnology Center (EGNC), Cairo University Sheikh Zayed Campus, 12588 Giza, Egypt.

* E-mail: m.abdelhamid999@gmail.com

Abstract. To improve the performance of organic solar cells by enhancing the properties of the photoactivated nanocomposite layer, the UV irradiation process was used to activate titanium dioxide nanoparticles (TiO_2 NPs). Herein, polymer solar cells were fabricated with FTO/(PAni-TiO_2)/Ag system. A series of mixed polyaniline (PAni) with 20% of activated TiO_2 NPs at different processing times was used to form PAni-TiO_2 nanocomposite films. The structural evolution, surface characteristics, optical and electrical properties of PAni-TiO_2 films have been investigated. XRD patterns showed that the UV treatment of TiO_2 NPs increased the crystallite from 18.35 to 24.1 nm and the degree of crystallinity increased by 5.6%. The irradiated PAni-TiO_2 films showed a rougher and more porous surface compared to the untreated one. Moreover, the adhesion force and electrical conductivity of the treated nanocomposite films at 8 h improved to be 137 mN/m and 6.62 S/m, respectively. Incorporation of activated TiO_2 NPs exposure to UV for different times from 0 to 8 h with the PAni matrix enhanced the current density (J_{sc}) of PAni-TiO_2 based nanocomposite solar cells from 3.11 to 4.83 (mA/cm^2) and their efficiency from 0.33 to 0.85%. The increase in the solar cell efficiency is mostly ascribed to a structural change accompanied by a rapid increase in surface roughness, which led to a decrease in the reflected photons and thus an increase in the charge carriers produced. These results revealed the effect of surface UV irradiation of TiO_2 NPs on their structural properties and the electronic contact between PAni and TiO_2 NPs, which greatly influenced the amount of carrier transport within the PAni-TiO_2 composites.

Keywords: Titanium dioxide (TiO_2), Ultraviolet (UV) Activation, PAni-TiO_2 Nanocomposite Films, Electrical Conductivity, Hybrid Solar Cells.

1. Introduction

Metal oxide nanoparticles (NPs) used as effective materials for electronic applications owing to their nanometric size that brings unique physical, chemical, and biological characteristics. Among these, TiO_2, ZnO, ZnS, GO, CdS and Fe_2O_3 NPs are widely used and offer extraordinary potential candidates to remove toxic elements [1]–[3].

In particular, NPs of titanium dioxide (TiO_2) have attractive properties including high surface area, simplicity of synthesis, non-toxicity, cheap cost, excellent chemical stability and distinctive optical, electrical, and magnetic properties.

These characteristics make TiO_2 NPs suitable for various applications, such as solar-photovoltaic, water splitting, electrochromic devices, pigment, cosmetics and photocatalysis [4]. In addition to that, it can be used for energy storage, sensors, optics, piezoelectric, and biotechnology [4], [5]. As it is known, optimizing the crystal size and phase structure of TiO_2 NPs leads to control of the optical energy gap for specific kinds of applications. The energy band gap has values of 3.0 and 3.13 eV for rutile and brookite structure, respectively [6]. However, it was found to be higher than 3.1-3.2 eV for the anatase structure and therefore, it could be excited by ultraviolet (UV) irradiation ($\lambda <$ 380 nm) [7]. Various chemical and physical methods have been utilized for the preparation of TiO_2 NPs such as solvothermal, sol-gel, sonochemical, hydrothermal, chemical vapor deposition (CVD), physical vapor deposition (PVD), electro-deposition, etc. [8]. Activation by UV irradiation is one of the promising methods that control the surface area, crystallinity, and morphology of TiO_2 nano-powder, which leading to enhance its physical properties [9]. For example, by applying high energy UV irradiation on anatase TiO_2 NPs enhances charge carrier transport or photoresponsivity. This is achieved through generating electron-hole pairs that in turn generate active free radical species, which can interact with the polymer matrix [9], [10].

The UV treatment has been employed to enhance the electrocatalytic activity of TiO_2 nanotubes. The UV treated TiO_2 nanotubes, revealed superior electrocatalytic activity that ascribed to the enhanced donor density and conductivity which in turn attributed to the formation of Ti^{3+} and oxygen vacancies [11]. Moreover, the UV treatment process is often performed to improve surface hydrophilicity and wettability [12]. Besides, UV irradiation has a great impact on the microstructure, wettability, optical behavior and electrical conductivity of TiO_2 thin films [4].

On the other hand, conjugated polymers are widely used in various applications due to their good physical, mechanical, chemical and electrical properties [13]. Unlike other conductive polymers such as polypyrrole and polythiophene, the conductivity of PAni varies from semiconductor to metal conductivity; and it can be easily controlled by modifying the mixing level [14]. Besides, PAni possesses many other attractive properties such as positive temperature coefficient of resistance (PTCR), photoelectric properties, easy and inexpensive to synthesize, multicolor electrochromic, and chemical sensitivity. Therefore, PAni can be used in numerous applications such as photovoltaic (PV) cells, gas sensors, anticorrosion coating, and tissue engineering [14], [15].

Recently, the inorganic materials composition and conducting polymers have great interests as merits that can be combined to achieve a final composite with good performance [16]. Previous studies have approved that the physical and chemical properties of PAni-TiO_2 nanocomposite differ completely from pure PAni and TiO_2, due to a strong chemical interaction between the components [16]–[18]. Unlike the individual components, PAni-TiO_2 nanocomposites exhibit high electrical conductivity properties [19]. Moreover, TiO_2 molecules can accumulate significantly in aprotic solvents; as a result, both the depth of light penetration and the surface area of TiO_2-polymer interface will be reduced.

As it is known, UV irradiation has been extensively widely used to activate TiO_2 NPs to for use as effective water purification catalysts. Herein, based on our knowledge, this is the first time to use UV irradiated TiO_2 NPs with improved electrical conductivity in synthesizing a high-performance nanocomposite layer for bulk-heterojunction (BHJ) organic solar cells. In order to evaluate the effect of using UV irradiated TiO_2 NPs on the properties of PAni-TiO_2 nanocomposite films, the microstructure, surface morphological analysis and properties of the synthesized films were considered and characterized. Further, the film optical and electrical properties were investigated and discussed. Accordingly, to assess the performance of PAni-TiO_2 nanocomposite layers that used different irradiated TiO_2 NPs, typical solar cells were fabricated. The J-V characteristic curves were measured in dark and under simulated sunlight with a total light intensity of 100 mW/cm^2 to estimate the solar cell efficiency.

2. Experimental procedures

2.1. Reagents and Materials

Titanium tetrachloride ($TiCl_4$), which supplied by Loba (purity: 99.5%), was used as raw materials for TiO_2 NPs preparation. Moreover, aniline monomer C_6H_7N (purity: +99%), hydrochloric acid HCl (concentration: 37%) and ammonium peroxydisulfate (APS) $(NH_4)_2S_2O_8$ were used to prepare PAni. All chemical materials were purchased from Sigma Aldrich.

2.2. Preparation of TiO_2 nanoparticles

30 mL of $TiCl_4$ was added to 300 mL of distilled water in a flask surrounded by an ice bath to prevent TiO formation and then, the mixture was placed on a magnetic stirrer (1000 rpm). The chemical reaction of the solution was kept at this condition for 1h then, the solution temperature raised to 70 ˚C for 2 h using a hotplate. After 3 days, the obtained suspension was washed several times with distilled water and thus, dried at a temperature of 70 ˚C. Finally, it was calcined at 450 ˚C for 3 h.

For UV treatment, the obtained TiO_2 NPs were activated under UV lamp at a wavelength of 364 nm and a working power of 15 W at different times of 2, 4, 6, 8, and 10 h. The distance between the TiO_2 NPs and the UV source 10 cm.

2.3. Synthesize of PAni-TiO_2 nanocomposites films

Chemical oxidative polymerization method was used to prepare PAni-TiO_2 nanocomposites, where the aniline monomer polymerized in the presence of HCl and ammonium persulfate (APS) as a catalyst and a strong oxidizing agent, respectively. APS is a colorless inorganic salt, highly soluble in water, which has a chemical formula of $(NH_4)_2S_2O_8$. The experimental method and reaction mechanism between the activated TiO_2 NPs and the aniline monomers for the formation of PAni-TiO_2 nanocomposites are illustrated in Fig. 1 and Fig. 2, respectively.

A 0.01 mol of aniline monomer is dissolved in a 0.01 mol of HCl acidic solution and mixed using an ultrasonic unit (Elmasonic S 40H) at room temperature. In another beaker, A 0.01 mol of APS was dissolved in 15 mL distilled water to prepare a dilute APS solution. To cover the TiO_2 NPs with conductive PAni as a shell, TiO_2 powder was dispersed in the beaker containing aniline monomer and placed on a magnetic stirrer for 30 min. TiO_2 solution was mixed to the aniline mixture with ratio 20% vs. 80% aniline solution followed by several minutes in the ultrasound to confirm the complete interaction between aniline and TiO_2 NPs. A dilute APS solution was placed into a burette and was slowly added dropwise to the mixture of aniline–HCl–TiO_2 under magnetic stirring (1000 rpm) in an ice bath at a reaction time of 5.5 h. Accordingly, the formation of PAni-TiO_2 nanocomposites can be performed using a modular physicochemical technique [20], which begins with a slow drop rate at approximately one drop/second and continues under stirring to ensure good oxidization and homogenous polymerization of the PAni solution. The color is observed to be changed to dark green at the end of physicochemical reaction. This indicates that an oxidation process is underway, which ends with the formation process composite solution of PAni-TiO_2 nanocomposites. Then, the precipitate was filtered and washed with distilled water and ethanol to remove excess acid. The final composites solutions were deposited by a spin coating process on FTO substrates at 800 rpm for 30 s followed by drying at 50 ˚C for 30 min. The deposition and desiccation processes were carried out in the air atmosphere. The same process was repeated by adding activated TiO_2 NPs at different exposure times (2, 4, 6, 8 and 10 h).

On the surface of TiO_2-NPs various hydroxyl groups are present. The reaction between H_2 bond and ethanol on the TiO_2 surface weakens the agglomeration of TiO_2. Then the aniline solution disperses the TiO_2 NPs properly. The chemical bond formed between TiO_2 and PAni during the polymerization process is stronger than the H_2 bond between the TiO_2 surface and the ethanol hydroxyl group [21].

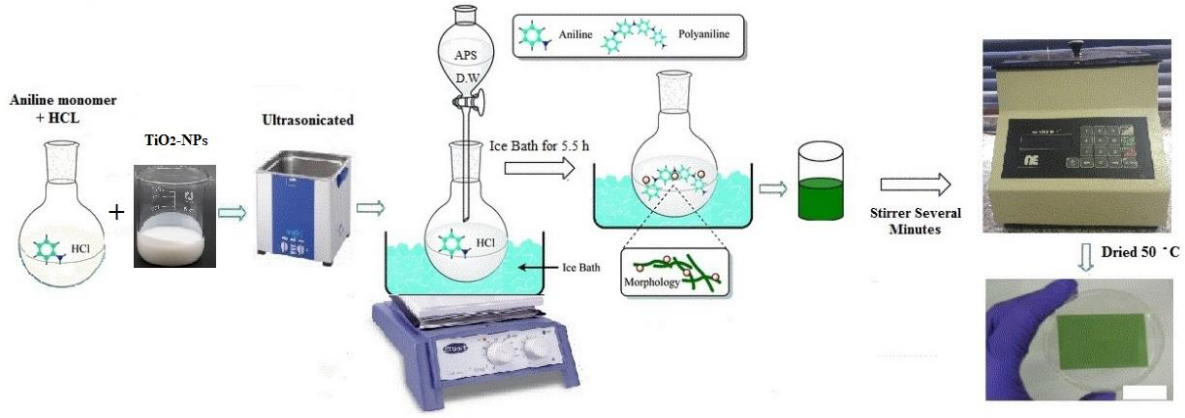

Figure 1. Experimental procedure for the synthesis of the Pani-TiO_2 nanocomposite

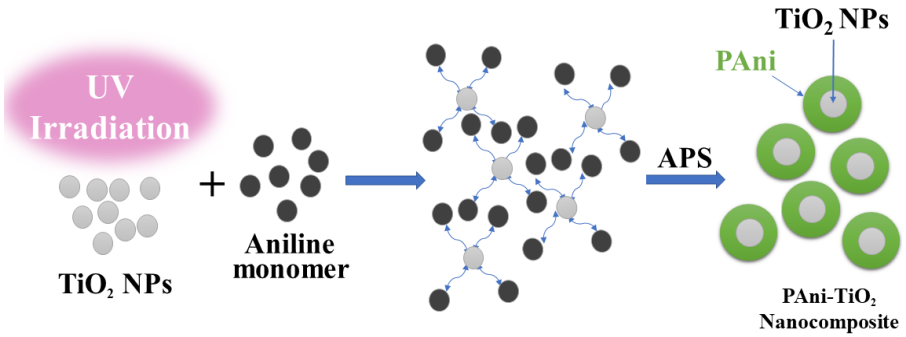

Figure 2. The reaction mechanism between the activated TiO_2 NPs and the aniline monomers for the formation of PAni-TiO_2 nanocomposites

2.4. Fabrication of FTO/PAni-TiO_2/Ag solar cell devices

Fluorine-doped tin oxide (FTO) (80-82% transmittance and 4 x 10^{-5} Ω.cm resistivity, sigma Aldrich) coated glass thin film was used in the fabricated organic solar cell devices as a transparent conductive anode. A metallic silver (Ag) paste (high concentration ≥75%, low resistivity of 1-3 x 10^{-5} Ω.cm) conductive material is used as a highly effective cathode. The FTO glass substrate is exposed to a special cleaning procedure using a dilute acidic solution of HCl followed by an extensive water rinse to remove the residual HCl. After that, it is sonicated in acetone from the surface of the conductive side, wet cleaned in ethanol and sonicate to remove organic impurities and finally rinse with deionized water. Then, the nanocomposites of PAni-TiO_2 as a photoactive layer is spin-coated on FTO surface. Finally,

high quality silver bus bars as a cathode were printed on the top surface of the PAni-TiO_2 nanocomposite using a screen printer coater (EQ-SPC-2-LD). A schematic of the stack device architecture is shown in Fig. 3.

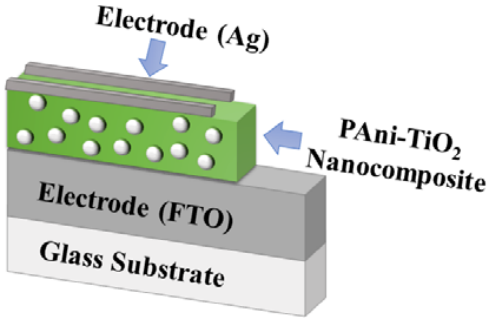

Figure 3. Organic solar cell architecture of FTO/PAni-TiO_2/Ag.

3. Characterization techniques

The X-ray Diffractometry (XRD) with a Cu target (Model D8 ADVANCE from Bruker) has been used to investigate the phase purity and structure of the prepared samples. The functional groups of TiO_2 NPs, pristine and treated nanocomposite thin films are evaluated using Fourier Transform Infrared (FTIR) Spectroscopy (Jasco Model 4100_Japan). The FTIR analysis is obtained from 4000 to 400 cm^{-1} with a resolution of 4 cm^{-1} at room temperature. The morphology of the obtained pure PAni and nanocomposite films was characterized by a high-resolution scanning electron microscope (SEM) (JOUL, JSM-5500, Japan) at an accelerated voltage of 10 KV. The optical properties of the nanocomposite films were evaluated using a computerized SPECORD 200 PLUS analytic Jena spectrophotometer with 1 nm step at normal incidence of light in the wavelength range of 190 – 1100 nm. An SEO Phoenix 300 contact angel analyzer was employed to measure the contact angle, wet energy, surface tension, diffusion of power factor and adhesion force. The surface roughness (Ra) was evaluated using a profilometer (Talysurf 50-Taylor Hopson precision). The electrical resistivity was measured with the four-point probe method using an EQ-JX2008-LD resistivity tester. The average electrical resistivity of each film was calculated from 10 reading sgained from various parts. Furthermore, the J –V characteristics of the solar cell under a fixed illumination intensity of 1.0 Sun at 25 ˚C is measured using a solar simulator system. The simulation test carried out in dark and illumination under standard condition (AM 1.5 G, 100 mW/cm^2) using a xenon lamp as a simulated light source irradiation with the use of a KEITHLEY 2400 Source Meter.

4. Results and Discussion

4.1. X-Ray Diffraction (XRD) Analysis

Fig. 4 shows typical XRD patterns of TiO_2 NPs, pure PAni, and PAni-TiO_2 nanocomposite films that treated by UV rays at different processing times, 2, 4, 6, 8 and 10 h, in compared to the untreated one. In all samples, peaks of diffraction intensities and widths are detected between 10˚ and 80˚ due to the parallel and perpendicular periodicity of the polymer (PAni) chain [22]. The structure of TiO_2 NPs primarily exists in three-phases: anatase, brookite, and rutile. Despite the rutile phase is highly persistent as bulk materials, preparation methods that include up to 450 ˚C are mostly

produce in favor of anatase structure [23]. Anatase phase is the most active catalytic phase among all of the other TiO_2 phases, as its surface energy is lower compared to the rutile and brookite phases [23]. Herein, the diffraction peaks of TiO_2 are in a good agreement with the tetragonal TiO_2 phase with anatase crystal phase (a = b = 3.7335 Å, c = 9.3788 Å, α = β = γ = 90.0) (ICSD, Code no 9852) [24]. Moreover, the diffraction peaks of the pure PAni are in a good agreement with the orthorhombic PAni structure (a = 7.3574 Å, b = 6.9675 Å, c = 10.1714 Å, α = β = γ = 90.0) [25], [26].

The diffraction peak at 2θ of 23˚ is due to polymer chains placed parallel and closed to each other producing crystalline zones surrounded by amorphous areas [27]. The polycrystalline diffractions of the untreated and UV-treated PAni-TiO_2 nanocomposite films are identical to those caused by the standard powder diffractions of tetragonal anatase TiO_2 structure and orthorhombic PAni. This indicates that no phase transformation involved in the UV activation process. Further, the peaks intensity of the nanocomposite films is strongly influenced by UV radiation, where it gradually decreases with increasing the processing times. These results may be attributed to the improvement in the physicochemical interaction between the activated-TiO_2 NPs and PAni with an increase in the UV irradiation time. Besides, the peaks corresponding to the planes (211), (221) and (201) are slightly shifted towards a lower degree of 2θ. These little changes revealed that UV radiation does not affect the lattice structure of PAni-TiO_2 nanocomposite films. Moreover, by increasing the processing times, (323) PAni peak and (323), (103), (112), (213), (204) and (116) TiO_2 peaks have gradually vanished from the patterns of the treated PAni-TiO_2 films that attributed to the restrictive effect of the surface of TiO_2 nanoparticles which increases under UV light [7].

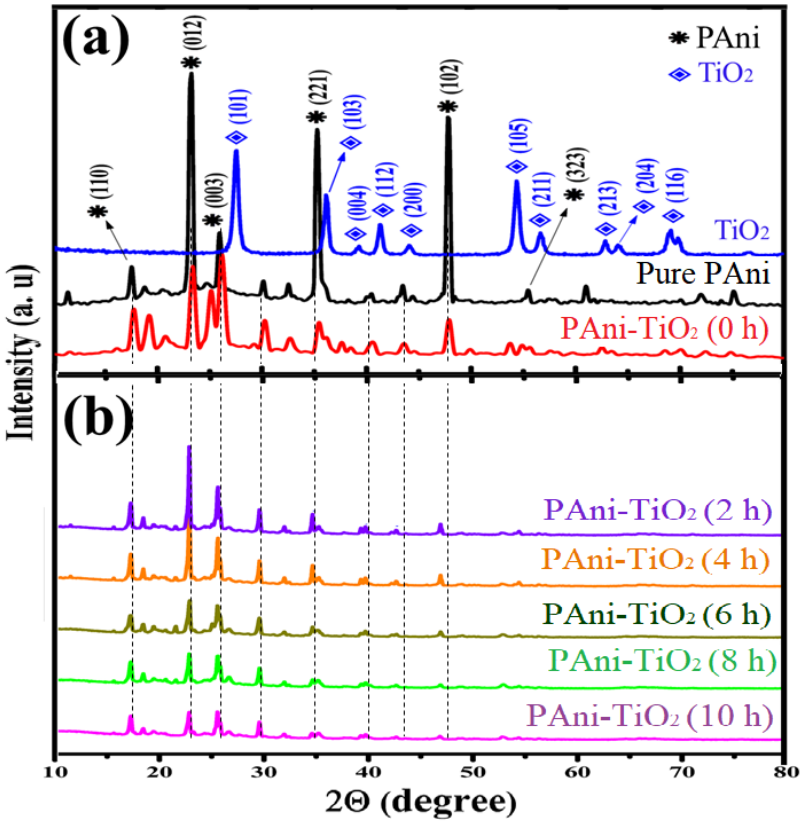

Figure 4. (a) XRD patterns of TiO_2 NPs, pure PAni and untreated PAni-TiO_2 nanocomposites films, (b) treated PAni-TiO_2 nanocomposites films synthesized of pure PAni with 20% of TiO_2 powder treated under UV light at processing time from 2, 4, 6, 8 and 10 h.

In general, crystallinity depends on the periodicity, that is the long-range order of atoms, ions or molecules in a particular sample. XRD patterns demonstrate that UV treatment has improved the crystallization of nanofilms as shown in Table 1. The XRD studies revealed an increase in the crystallinity of PAni-TiO_2 treated films compared to the untreated one. The crystallinity increased from 79.7% for the untreated film to 86.2% for one treated at 10 h processing time.

The crystallite size (D) can be calculated from the average of all main peaks using the Debye–Scherrer equation [28]:

$$\boldsymbol{D = \frac{0.94\,\lambda}{\beta\, cos(\theta)}} \qquad \textbf{(1)}$$

Where **λ** is the wavelength, **β** is the full width at half maximum of the peak, and **θ** is the diffraction angle. The crystallinity and the crystallite size of pure-TiO_2 NPs are 80.6% and 18.35 nm, respectively, as shown in Table 1 and gradually increased as the duration of exposure to UV compared to pristine PAni-TiO_2 nanocomposite. This can be attributed to the UV radiation that strongly affects the TiO_2 surface leading to different interactions between PAni and TiO_2 in the nanocomposite films and also attributed to the physical dependence of the polymer on the TiO_2 NPs surface.

Table 1. Crystallite size and crystallinity of UV treated and untreated PAni-TiO_2 nanocomposite samples

Sample	Crystallite size (nm)	Crystallinity (%)
TiO_2 powder	18.35	80.6
Pure PAni	22.39	77.3
PAni-TiO_2 (0h)	20.21 – 2	79.7
PAni-TiO_2 (2h)	21.51	83.4
PAni-TiO_2 (4h)	22.20	83.5
PAni-TiO_2 (6h)	23.42	83.7
PAni-TiO_2 (8h)	23.76	84.5
PAni-TiO_2 (10h)	24.10	86.2

4.2. FTIR Spectra

FTIR spectra was obtained in order to confirm the interaction formulation of the chemical compounds that formed between TiO_2 NPs, pure PAni to form PAni-TiO_2 nanocomposite as seen in Fig. 5. Three main absorption bands are observed in TiO_2 NPs sample. The first peak is appeared at 3437 cm^{-1} and it belongs to stretching vibrations hydroxyl (O–H), representing the water as moisture. The second peak is observed at 1627 cm^{-1}, and it belongs to stretching Ti–O bond [29]. The third one in a broad and strong peak between 800–450 cm^{-1} is assigned to vibrations in the stretching Ti–O–Ti bonds [30], [31]. In case of the PAni-TiO_2 nanocomposite, the main peaks of pure PAni bands continue to appear clearly in a nanocomposite in the region 3139–472 cm^{-1} with intensity changes and a small peak shift towards higher wavenumbers, which assigned to the presence of TiO_2-NPs in the nanocomposite structure. The absorption peak between 3690–2983 cm^{-1} can be attributed to the stretching of O–H and hydrogen-bond N–H stretching of aromatic amine [32], [33]. Surfaces of the hydroxyl bonds can accept photo-induced holes and form hydroxyl radicals [34]. As a result, these radicals can improve the photocatalytic activity of the composite [35]. The characteristic peaks at 1537 cm^{-1} and 1412 cm^{-1} are assigned to C=N and C=C ring asymmetric and symmetric stretching vibrations, due to the presence of quinonoid structures and benzenoid ring, respectively. The peak at 1301 cm^{-1} corresponds to C–N stretching of the benzenoid unit. The peak at 1193 cm^{-1} is due to the quinonoid unit of the PAni doped, which is used to measure the degree of delocalization and is characterized as the peak of the PAni conductivity [36]. The existence of the main peaks of PAni (i.e. C=C and C–N peaks) in the spectrum of PAni-TiO_2 nanocomposite confirmed the formation of PAni on nano TiO_2 surface [7]. The peaks at 870-743 cm^{-1} are associated with C–C and C–H in the benzenoid unit [20]. Whereas, the peak at 616 cm^{-1} is relatively enhanced compared to pure

PAni, which may be attributed to the out-of-plane bending flexural vibration of C—H aromatic rings of PAni and vibrations in the stretching Ti—O—Ti bonds of TiO_2 [32].

According to the results, the peak appears at 3193 cm^{-1} in a nanocomposite characterized by high intensity, wide stretching shape and small shifting towards short wavenumber compared to that found in pure PAni. This might be attributed to the attraction by a group of adjacent atoms or two nearby functional groups [37]. Moreover, the decrease in the intensity of the characteristic peak at 616 cm^{-1} for TiO_2-NPs compared to the corresponding finger peak in the PAni-TiO_2 nanocomposite indicates a structural change in the polymer matrix resulting from a strong H-bonding interaction exists between PAni and TiO_2-NPs. The good interaction of PAni to TiO_2-NPs surface led to shield the nanoparticles with a coating PAni layer due to coordination between the N atoms of the PAni chains and the TiO_2 NPs [38], [39].

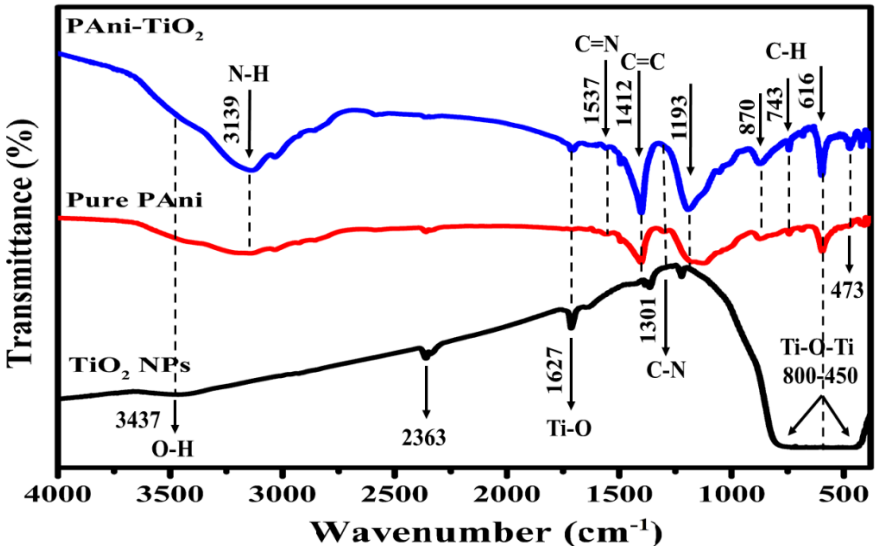

Figure 5. FTIR spectra of TiO_2-NPs, pure PAni and PAni-TiO_2 nanocomposite

4.3. Morphology

SEM images of pristine TiO_2, pure PAni, untreated and treated PAni-TiO_2 composite films are shown in Fig. 6. From the SEM micrographs, a porous topography of pristine TiO_2 and pure PAni is observable. Based on the previous literature, the increased active layer with a microporous structure results in a relatively rough surface, which increases the surface contact between the nanocomposite layers and the electrode surface [40]. In the microporous surface of the active layer of the composite, the increased capacitance can take place as a result of maximum absorption [41]. Moreover, pristine and activated TiO_2 NPs are dispersed in a PAni matrix showing a thick film integrated with featured structure and non-agglomerated TiO_2 NPs [27], [42]. This could be attributed to the formation of PAni shell on the surface of TiO_2 NPs that causes repulsion forces between nanoparticles preventing their agglomeration [41]. The morphology of the nanocomposite particles depends on the conditions of polymerization such as pH, temperature, polymerization time as well as the TiO_2 structure and ratio [43]. Besides, the white area is assigned to be TiO_2, while the grey and black areas refer to the polymer chain. By increasing the processing time from 0 to 8 h (Fig. 6b-g), the activated PAni-TiO_2 films showed improvement in the white surface area distribution compared to the untreated one. This may confirm that the activated TiO_2 is distributed uniformly over the surface of the polymer molecules with increased activation time. Furthermore, the formation of nanoflakes in the nanocomposite structures was observed for samples containing TiO_2 NPs that were exposed to UV radiation for a relatively long period of time 8 and 10 h (see

Fig. 6g and 6h) [40], [41]. This morphological phenomenon can be attributed to the improvement in the physicochemical reaction between the activated TiO_2 and PAni.

Increasing the processing times results in a significant improvement in the crystallization of the nanoparticles and reactive surface area with PAni chains. Moreover, the agglomerating aspect vanishes as activated-TiO_2 NPs, and well distributed on the long PAni chains; causing a repulsive action preventing agglomeration process. This leads to creating a morphological structure with nanoflakes. As the UV irradiation times of TiO_2 NPs increase, the adsorptive properties of the PAni matrix increase and the surface area for nanoflakes increases. These nanoflakes improve the efficiency of electrical properties and photocatalytic activity [21].

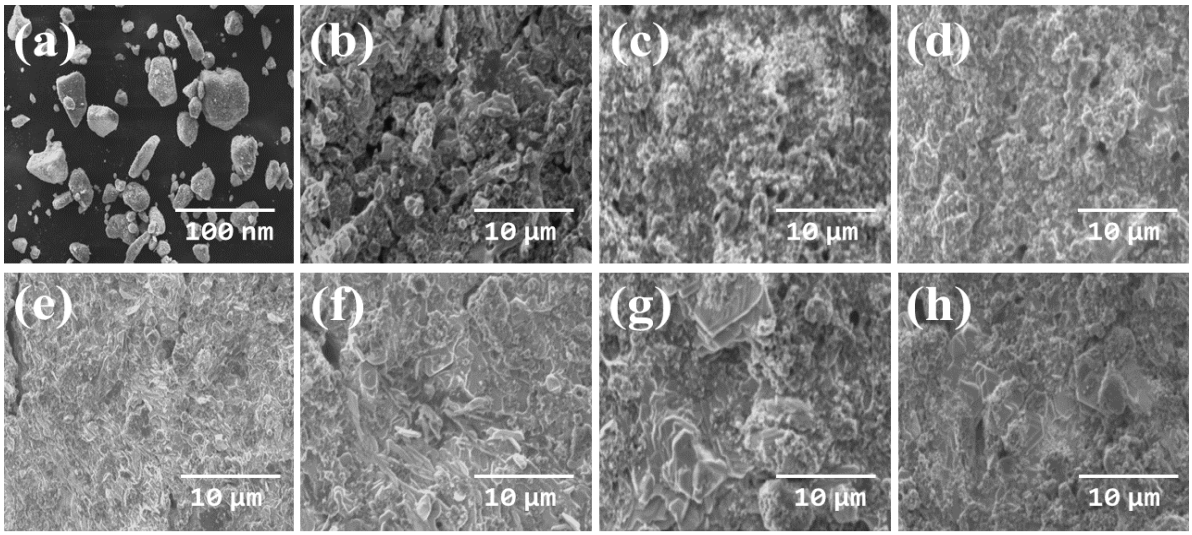

Figure 6a-h. SEM images of a) Pristine TiO_2 NPs, b) Pure PAni film, c) Untreated PAni-TiO_2 nanocomposite film, d:h) PAni-TiO_2 nanocomposite films of treated TiO_2 powder by UV at 2, 4, 6, 8 and 10 h, respectively, at fixed mixing ratio of 20% TiO_2 NPs.

4.4. Optical Properties

The optical properties of pure PAni film and PAni-activated TiO_2 nanocomposite films as a function of UV treatment time has been investigated and discussed. Fig. 7a,b reveals the absorbance and transmittance spectra of all films at near-normal incidence over a wavelength range of 300–800 nm. Fig. 7a shows a similar spectrum of broad absorption peaks in the range of 325–465 nm and 550–800 nm for pure PAni and nanocomposite films with absorption peak shifts. The absorption band of 550–800 nm shifts towards lower wavelengths with increasing the UV irradiation time of the TiO_2 NPs up to 8 h. This band shift indicates the effect of activated TiO_2-NPs on electronic structure of TiO_2 NPs in valence band that could interact with the higher occupied molecular orbital (HOMO) of the PAni [21]. On the other hand, increasing the processing time to 10 h leads to a different behavior where a small shift towards the higher wavelengths occurs. These shifts indicate the formation of nanocomposite with TiO_2 [44]. Pure PAni shows as an energy absorption equivalent at wavelengths of 330, 420 and 600 – 800 nm which in turn leads to transitions of $\pi \rightarrow \pi^*$ within the benzenoid rings, Polaron$\rightarrow\pi^*$ of quinoid rings, and $\pi \rightarrow$polaron excitonic of the quinoid rings, respectively [45]. These observed peaks gradually increase in intensity with a slight shift towards higher wavelengths in the PAni-TiO_2 nanocomposites. This confirms the formation of the polaron tape in the bandgap of the PAni and was strongly influenced by the incorporation of treated TiO_2 NPs. A peak is also observed around 690 nm for pure PAni which correlates to the benzenoid and quinoid excitonic transition.

A minimum absorption peak is mostly observed for untreated PAni-TiO_2 nanocomposite (at 0 h). Thereafter, absorption was gradually increased as the UV radiation treatment times increased to reach the optimum value at 8 h of treatment. This can be attributed to the good interactions between PAni and TiO_2 NPs [46]. The same behavior for PAni-TiO_2 absorption curve has been previously observed [47], [48]. It is well known that PAni-TiO_2 nanocomposites

display applications on a large scale for photocatalytic when they have good absorption in the ultraviolet spectrum range [47].

In general, the transmittance spectra of PAni-TiO_2 nanocomposite films are strongly different depending on the UV light treatment time. The maximum transmission has been detected at the pristine TiO_2 NPs and, hence, gradually decreased with increasing the treatment time to have the lowest value at a treatment time of 8 h. This corresponds to π-π* transition in the UV and bipolaronic band in the visible regions.

The optical band gap *(E_g)* of the samples can be calculated using the universal method, Tauc relationship, for direct allowed transition semiconductor materials [49].

$$\boldsymbol{\alpha h\nu = B\left(h\nu - E_g\right)^{1/2}} \qquad \textbf{(2)}$$

Where $\boldsymbol{h\nu}$ is photon energy and $\boldsymbol{B}$ is a parameter which is related to the transition probability, $\boldsymbol{\alpha}$ is the absorption coefficient and $\boldsymbol{E_g}$ is the optical band gap [50]. The E_g values are directly related to the film composition and structure. On the other hand, it has been found that its value increased with increasing the time of exposure to UV rays of TiO_2 powder as it is listed in Table 2. These values are higher than that calculated value for the unmodified PAni-TiO_2 (1.65 eV). The optical absorption has found to be dependent on the short-range order in the amorphous state and defect state [51]. In the present system, the increased of the optical band gap might be attributed to the reduction of the system disorder and the increase of the defect state density. Tone can conclude that introducing treated TiO_2 into the PAni has a potential effect on the optical properties of active nanocomposite films.

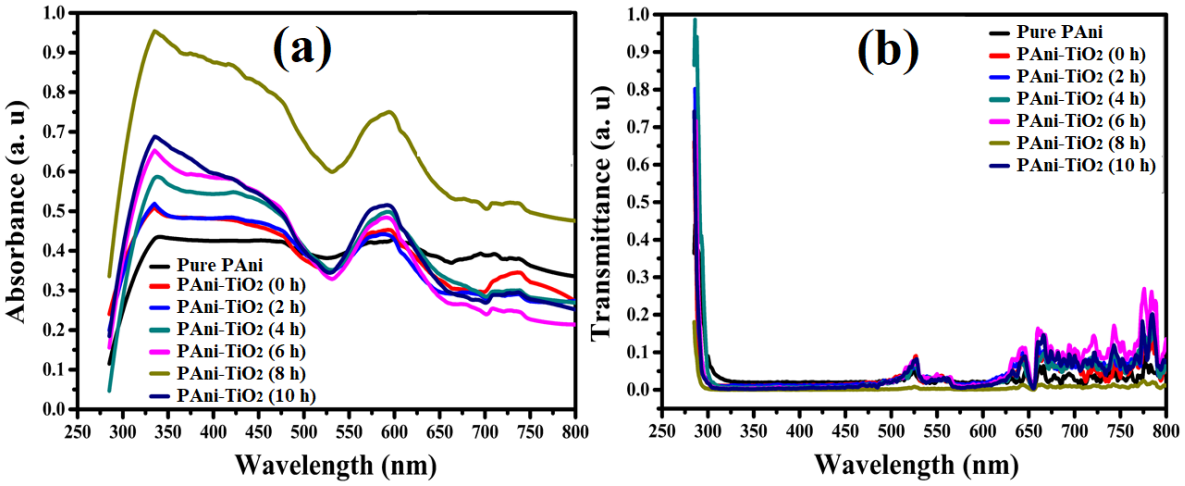

Figure 7a,b. a) absorbance, b) transmittance for pure PAni, pristine and modified PAni-TiO_2 nanocomposites using UV irradiation for TiO_2 powder at various times.

Table 2. Energy band gap values of the obtained nanocomposite films treated at different times

Treatment Time (h)	Pure PAni	PAni-TiO_2 (0 h)	PAni-TiO_2 (2 h)	PAni-TiO_2 (4 h)	PAni-TiO_2 (6 h)	PAni-TiO_2 (8 h)	PAni-TiO_2 (10 h)
Eg (eV)	2.26	1.65	1.77	1.76	1.87	1.99	1.65

4.5. Water droplet interaction with PAni-TiO_2 nanocomposites

The contact angles (CAs), adhesion force, wettability, and water droplet spreading coefficient on the surface of PAni-TiO_2 nanocomposite films were strongly affected by the activation degree of TiO_2 using UV rays as shown in the Fig. 8a-d. The CA of the untreated PAni-TiO_2 film was approximately 52.81˚, which gradually decreased to be 46.07˚, 36.02˚, 32.96˚, 27.46˚ after UV treatment time of 2, 4, 6 and 8 h, respectively. This indicates that the PAni-TiO_2 nanocomposite films are highly hydrophilic. Then, the CA value increased to 31.39˚ after UV treatment time of 10 h as shown in Fig. 8a. The fundamental explanations of the observed difference confirm the great influence of the crystallite size, molecular interactions [51], [52], and vertical topographical variation (roughness) on the electrochemical properties of PAni-TiO_2 surfaces [53], [54]. While the CA value was gradually decreasing, the work of adhesion was increased by increasing the treatment time to achieve the optimum value of 137.39 mN/m at a treatment time of 8 h, as shown in Fig. 8b. The work of adhesion
presents the adhesion force between obtained films and droplet water, and it can be calculated from the next equation [55]:

$$W_{sl} = \gamma_s + \gamma_l + \gamma_{sl} \qquad (3)$$

where γ_s, γ_l, and γ_{sl} are the surface free energies of solid, liquid (water in this study), and solid-liquid interfacial energy, respectively. Combining this equation with the next equation of Young-Dupré

$$\gamma_s = \gamma_{sl} + \gamma_l \cos \theta_e \qquad (4)$$

We got [56]:

$$W_{sl} = \gamma_l (1 + \cos \theta_e) \qquad (5)$$

where θ_e is the equilibrium (Young's) contact angle between PAni-TiO_2 nanocomposite films and water, and γ_l is the water surface tension on the solid surface.

An examination of the interaction of a water drop with the modified TiO_2 nanostructured surfaces within PAni chains reveals that the water absorption on the nano-surface depends on the density of the surface charge, which is strongly affected by the nanoscale roughness and the surface physicochemical properties (among them wettability) [57]. The wettability and spreading coefficient of PAni-TiO_2 films showed that they are highly dependent on the modification time and the drop retraction due to the hysteresis of contact angles from rough surfaces, as seen in Fig. 8c,d [58]. The same behaviour was reported on PAni-TiO_2 nanocomposite films [59].

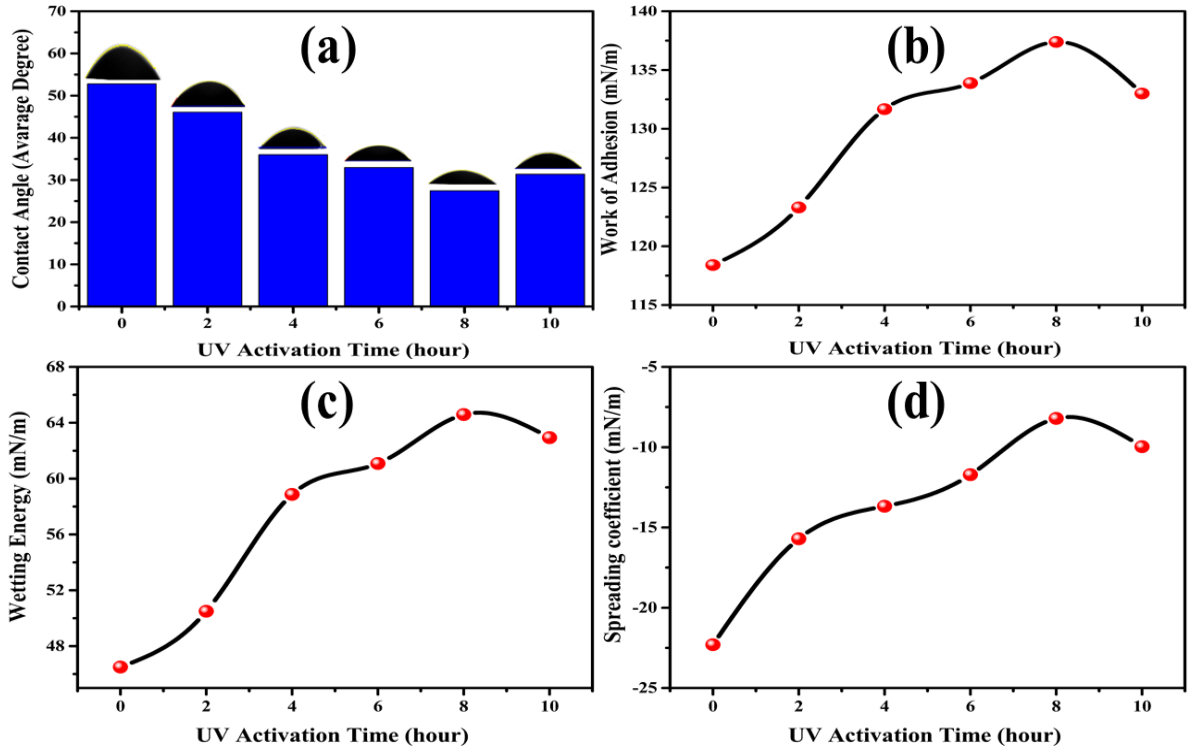

Figure 8a-d. a): Contact angle, b) adhesion force, c) wetting energy, d) spreading coefficient for pristine and modified PAni-TiO_2 nanocomposites using UV irradiation for TiO_2 powder at various times.

4.6. Roughness Measurements of PAni-TiO_2 Nanocomposite Films

Roughness measurements of nanofilms, consisting of the PAni matrix and activated TiO_2 NPs at different times under a UV lamp, revealed a great diversity. Fig. 9 shows the measured factors of surface roughness, i.e. average roughness (Ra) and root mean surface roughness (Rq). It was found that Ra and Rq have values of 2.74 and 3.72 μm, respectively for the untreated film. These values increased to the maximum values of 5.04 and 6.38 μm, for Ra and Rq, respectively with increasing the activation time to 8 h. Then, it decreased to 3.01 and 3.9 μm after 10 h of UV treatment time. The interpretation of this dissimilar trend is mostly ascribed to the difference in the structural features of both nanocomposites. The effect of molecular interactions, crystallite size of the irradiated-TiO_2 NPs within PAni matrix and their distribution over the long PAni chains leads to an increased surface roughness [51], [60]. However, the fibrous network structure is mostly responsible for surface smoothness. It fully agrees with the contact angle results. The change in the surface roughness of the nanocomposite films affects their optical properties including transmittance, absorbance and optical constants [61].

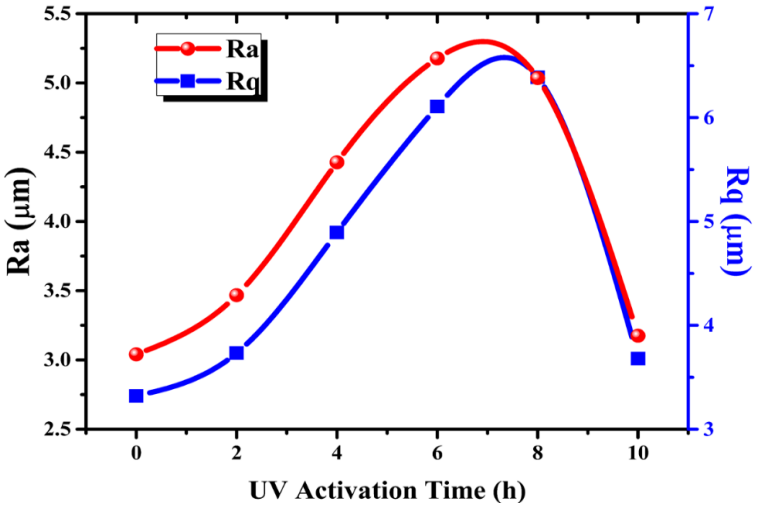

Figure 9. The surface roughness parameters for pristine and modified PAni-TiO_2 nanocomposites using UV irradiation for TiO_2 powder at various times.

4.7. Electrical Conductivity of PAni-TiO_2 Nanocomposite Films

The prolonged UV-activation process can enhance the catalytic and electrical properties of TiO_2 through holes induced by ultraviolet radiation and reducing the adsorbed oxygen by electrons, equation (6) [62].

$$TiO_2 + hv \rightarrow TiO_2 (h^+_{V.B} + e^-_{CB}) \quad (6)$$

Subsequently, PAni electrical properties can be enhanced by adding activated TiO_2 NPs inside the PAni chains [63]. Interaction between O^- ions on the surface of TiO_2 grains and the nitrogen atoms in the large PAni molecules causes electrons trapping by releasing the oxygen ions and returning to the surface of the grains [64].

The electrical properties of the obtained pure PAni and PAni-TiO_2 samples were investigated. As seen in Table 3, the conductivity of the unmodified PAni and treated PAni-TiO_2 at different treatment times of 0, 2, 4, 6, 8 and 10 h under UV irradiation. Resistivity is measured by the 4PP (EQ-JX2008-LD) method and approved that; UV irradiation treatment has a significant effect on the electrical conductivity of the obtained films. As observed from the current results, the electrical conductivity of pure PAni film is 4.77 S/m and increases to 5.26 S/m in the untreated nanocomposite film. However, for the synthesized nanocomposite films based on the UV activated TiO_2 NPs at different times (2, 4, 6 and 8 h) leads to gradually enhance the conductivity of films to 6.11, 6.32 and 6.54 and 6.62 S/m, respectively. This behavior has been previously investigated by others and has been mainly ascribed to the physicochemical reactions of activated-TiO_2 NPs within the matrix structure; which leads to a change in the oxidation state [65], [66]. It is known that the difference in oxidation level of PAni inevitably affects its electronic structure. Accordingly, the polaron band has found to be smaller for pure PAni (corresponding to absorption spectra) than that of phase PAni in the pristine composites, and it was gradually improved by increasing the UV processing times of TiO_2 NPs [65]. This in turn leads to high mobility of charge carriers (polarons) along PAni chains [66]. These show higher values than that of previous studies such as SU Bitao et al ($2.86x10^{-7}$ S/m) [63] and Xingwei Li et al. ($2.9x10^{-7}$ S/m) [67]. This significant improvement in conductivity may arise due to the transfer of electrons from the surfaces of the polar O^{2-} TiO_2 NPs to the PAni chains, causing them to be reduced. In a highly reduced PAni, localized charges can be strongly obtained in a PAni ring [64].

A similar effect was obtained on modified TiO_2 films using UV irradiation and correlated with an increase of n-type conductivity due to the formation of lattice or electronic defects, like oxygen vacancies or interstitial Ti^{4+} ions [4], [61]. These results prove that focusing the UV rays on TiO_2 NPs surfaces, may realize more carries and electronic interaction between PAni and TiO_2 in PAni-TiO_2 composites that may increase electrical conductivity. Furthermore, increasing the activation process to 10 h decreased the conductivity value to be 5.88 S/m. This may be attributed to a relative increase in the segregation of PAni chains upon prolonged treatment, with a high agglomeration of TiO_2 inside the PAni matrix. This results in the formation of a non-conducting agglomeration zone in the PAni-TiO_2 layer, which in turn reduces carrier mobility and the electrical conductivity [62]. Also, many factors such as the mixing ratio of TiO_2 NPs within the polymer matrix may, increase the reaction of Pani-TiO_2 and reduction of the conjugated lengths in the PAni chains [57,58], and may also occur due to a fundamental network imbalance or TiO_2 nano purity [59], [64].

Table 3. Electrical conductivity behavior for pure PAni, untreated nanocomposite film and treated PAni-TiO_2 nanocomposite films using UV irradiation for TiO_2 NPs at various times

Treatment Time (h)	**Pure PAni**	**PAni-TiO_2 (0 h)**	**PAni-TiO_2 (2 h)**	**PAni-TiO_2 (4 h)**	**PAni-TiO_2 (6 h)**	**PAni-TiO_2 (8 h)**	**PAni-TiO_2 (10 h)**
Conductivity (S/m)	4.77	5.26	6.11	6.32	6.54	6.62	5.88

4.8. Performance evaluation of solar cells based on PAni-TiO_2 nanocomposite films

Current density–voltage (J–V) measurements were obtained for the fabricated solar cells in the dark and illumination states. I–V tester device was used in the presence of a simulated solar spectrum applying 1000 W/m^2 with standard conditions including air mass (AM) of 1.5 G and temperature of 25 ˚C. The current flows in the solar cell circuit and recorded as a function of applied voltage under the stimulated white- light illumination. Herein, PAni's hybrid photoactive layers were designed as a donor mixed with activated-TiO_2 NPs as acceptor in the fabricated solar cells. As observed in the J–V characteristic in dark, the test devices that were structured by pure PAni, pristine and treated photoactive layers exhibited the same asymmetric diode-like behavior as shown in Fig. 10.

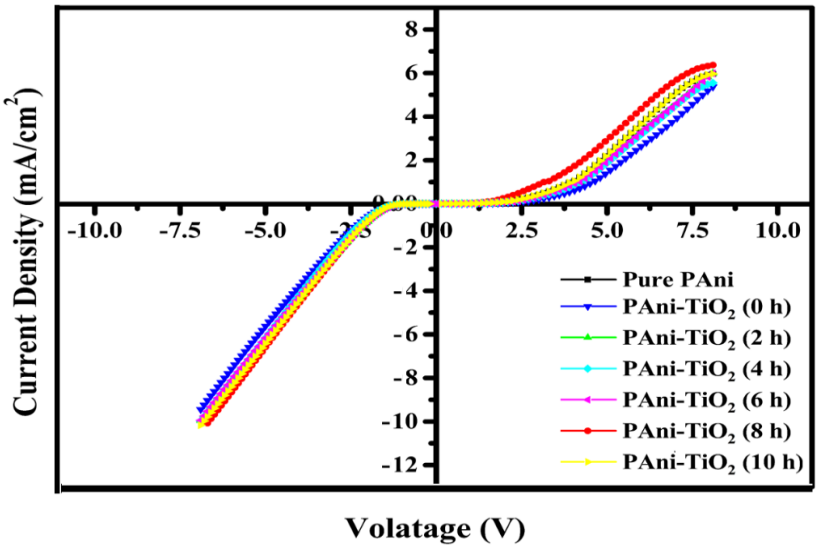

Figure 10. Diode-like behaviour of J-V curves obtained in the dark of designed photovoltaics based on pure PAni film, untreated nanocomposite film (pristine) and treated PAni-TiO_2 nanocomposite films using UV irradiation for TiO_2 NPs at different times (2, 4, 6, 8 and 10 h) as activate layers.

Incorporation of TiO_2 NPs within the PAni matrix increases the conductivity due to the contribution of polarons and bipolarons, which can move within shorter distances along polymer chains. Fig. 11 shows J–V curves of fabricated photovoltaic cells based on pure PAni, pristine composite and treated PAni-TiO_2 nanocomposites under illumination. As observed, the J–V curve is shifted towards higher values of current densities for the pristine composite device structured by FTO/PAni-TiO_2 (0h)/Ag compared to that one fabricated with FTO/pure PAni/Ag. These results indicate that incorporating of TiO_2 NPs within the PAni matrix significantly increases the carriers transport in the PAni structure by contributing to polarons and bipolarons, which move at shorter distances in polymer chains [68]. Moreover, incorporation of UV activated TiO_2 NPs at different processing times into the PAni-structure to form PAni-TiO_2 photoactive layer results in a gradual increase in current density values (J–V curves) compared to those designed with the pristine layer. The possible reason of the higher current density may be ascribed to (i) the increase in the physicochemical reactions between PAni and TiO_2 as well as the number of charge carriers that occurred by the activation process of TiO_2 NPs using UV irradiation at long processing times [69] (ii) a reduction in the interfacial resistance between TiO_2 and PAni owing to the increase in the number of polarons in PAni structure and the structural homogeneity of nanocomposites [70].

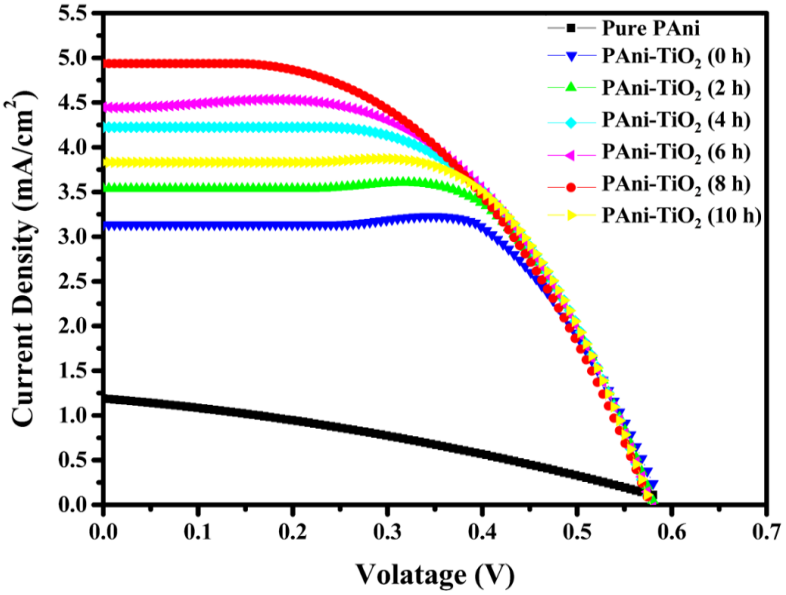

Figure 11. Illumination J-V characteristic curves of fabricated photovoltaic cells based on pure PAni, pristine composite and treated PAni-TiO_2 nanocomposites under simulated light irradiation 100 mW/cm^2 and AM 1.5 G.

Photovoltaic parameters of the solar cell device such as short circuit current density (J_{SC}), open circuit voltage (V_{OC}), fill factor (FF) and power conversion efficiency (η) can be attained from J–V characterization curves, as listed in Table 4. The V_{OC} is the voltage at the intercept of the J–V curve with the abscissa (horizontal axis) of the J–V diagram; whereas the J_{SC} is the value of current density at the intercept of the J–V curve with the ordinate (vertical axis). As observed, V_{OC} depends mostly on the trade-off energy between highest occupied molecular orbital (HOMO) of the donor and lowest unoccupied molecular orbital (LUMO) of the acceptor.

Herein, measurements of V_{OC} showed nearly constant values as the photoactive material (PAni) and have constant value (around 0.58 V) for all designed photovoltaic devices [71]. Moreover, it is known that the increase in J_{sc} relies mainly on the carrier's movement which includes generation, separations, transportation and collection on electrodes [72]. The photoactive layer modification process with UV-activated TiO_2 NPs plays an important role in improving short circuit current properties.

The photovoltaics efficiency of FTO/Pure PAni/Ag is 0.23% and increased to 0.33% by incorporating the pristine TiO_2 NPs into PAni structure. This is due to an increase of photocurrent density within composites structure [70]. The designed solar cells using activated-TiO_2 NPs exhibit a gradual improvement in the efficiency values of 0.42%, 0.55% and 0.69% at UV processing times of 2, 4 and 6 h, respectively. Then, it is increased to an optimum value of 0.85% for activated nanocomposite layer synthesized with a UV irradiated TiO_2 NPs for 8 h. All these manufactured devices show a better Performance based on their calculated efficiencies compared to that of other similar devices fabricated using of PAni-TiO_2 as active layers [69], [73], [74]. This performance improvement might be ascribed to the following reasons:

(i) At relatively high UV processing times, the physiochemical interaction between p-type PAni and n-type anatase-TiO_2 NPs can be increased and lead to an improvement in the donor/ acceptor interface that creates easy exciton dissociation [69].

(ii) The increase in the number of polarons and bipolarons in the PAni structure, which creates an efficient charge carries transfer network in the nanocomposite material. This interprets the conduction mechanism of the PAni-TiO_2 nanocomposite [75].

(iii) The rapid increase in surface roughness decreases the reflected photons and thus increases the produced charge carriers.

On the other side, prolonged processing time up to 10 h for TiO_2 NPs led to reduce the current density and cell efficiency to 3.81 (mA/cm^2) and 0.44%, respectively. This can be attributed to the reduction of exciton dissociation

resulted uneven distribution of TiO_2-NPs in PAni matrix along with uncontrolled aggregation for TiO_2 which can reduce the hole transportation [62].

Table 4. Characteristic parameters for pure PAni, pristine and modified PAni-TiO_2 nanocomposites solar cells

Sample	V_{oc} (V)	J_{sc} (mA/cm^2)	FF (%)	η (%)
FTO/Pure PAni/Ag	0.58	1.17	34.8	0.23
FTO/PAni-TiO_2 (0h)/Ag	0.58	3.11	18.0	0.33
FTO/PAni-TiO_2 (2h)/Ag	0.58	3.58	20.2	0.42
FTO/PAni-TiO_2 (4h)/Ag	0.58	4.17	20.8	0.50
FTO/PAni-TiO_2 (6h)/Ag	0.58	4.45	26.3	0.69
FTO/PAni-TiO_2 (8h)/Ag	0.58	4.83	30.3	0.85
FTO/PAni-TiO_2 (10h)/Ag	0.58	3.81	20.1	0.44

5. Summary and conclusion

TiO_2 NPs with anatase structure phase was successfully synthesized and then activated under UV irradiation at different exposure times for 2, 4, 6, 8 and 10 h. Activated-TiO_2 NPs was added during polymerization process of aniline monomers to synthesize highly conductive PAni-TiO_2 nanocomposites. Moreover, a PAni-TiO_2 nanocomposite solution was successfully obtained in a film form. The optical and electrical properties of the photoactivated PAni-TiO_2 nanocomposite films have found to be improved with increasing the processing times of the TiO_2 NPs. Further, the surface roughness and the porosity of the PAni-TiO_2 films were also increased. At UV irradiation time for TiO_2 NPs at 8 h, the crystallinity, optical energy gap and adhesion force of the PAni-TiO_2 nanocomposites were enhanced and found to be 86 %, 1.96 eV and 137 mN/m, respectively. Furthermore, the electrical conductivity of PAni-TiO_2 films was improved to 6.623 S/m after a UV treatment time of 8 h, where the transport of charge carriers in PAni-TiO_2 composites was increased. The current density (J_{sc}) of the PAni-TiO_2 nanocomposite based solar cells was increased from 3.11 to 4.83 (mA/cm^2) and the efficiency increased from 0.33 to 0.85% as the UV processing times of TiO_2 NPs increased from 0 to 8 h. This performance improvement may be ascribed to a structural effect along with the rapid increase in surface roughness which can decrease the reflected photons and thus increase the produced charge carriers.

References

[1] Lizama C, Freer J, Baeza J and Mansilla H D 2002 *Catal Today* **76** 235–246.
[2] Poulios I, Micropoulou E, Panou R and Kostopoulou E 2003 *Appl Catal B Environ* **41** (4) 345–355.
[3] El-Hossary FM, Ghitas A, Abd El-Rahman AM, Ebnalwaled AA, Fawey MH and Shahat MA 2020 *IOP Conference Series: Materials Science and Engineering* **762** 012001.

[4] Addonizio M L, Aronne A and Imparato C 2020 *Appl Surf Sci* **502** 144095.
[5] Hagfeldt A and Graetzel M 1995 *Chem Rev* **95** 49–68.
[6] Reyes-Coronado D, Rodríguez-Gattorno G, Espinosa-Pesqueira M E, Cab C, De Coss R d, Oskam G 2008 *Nanotechnology* **19** (14) 145605.
[7] Monfared A H, Jamshidi M, Hashemi Monfared A, Jamshidi M, Monfared A H and Jamshidi M 2019 *Prog Org Coatings* **136** 105257.
[8] Manjunath K, Yadav LSR, Jayalakshmi T, Reddy V, Rajanaika H, Nagaraju G, et al 2018 *J Mater Res Technol* **7** (1) 7–13.
[9] Zenteno A, Lieberwirth I, Catalina F, Corrales T, Guerrero S, Vasco DA, et al 2017 *Compos Part B Eng* **112** 66–73.
[10] Zapata PA, Rabagliati F M, Lieberwirth I, Catalina F, Corrales T 2014 *Polym Degrad Stab* **109** 106–114.
[11] Tian M, Thind S S, Dondapati J S, Li X, Chen A 2018 *Chemosphere* **209** 182–190.
[12] Banerjee S, Dionysiou D D, Pillai SC 2015 *Appl Catal B Environ* **176** 396–428.
[13] Najafi V, Ahmadi E, Ziaee F, Omidian H, Sedaghat H 2019 *J Polym Environ* **27** (4) 784–793.
[14] Saeed M, Shakoor A, Ahmad E 2013 *Polym Sci Ser A* **55** (9) 549–555.
[15] Kuwabata S, Takahashi N, Hirao S, Yoneyama H 1993 *Chem Mater* **5** (4) 437–441.
[16] Gangopadyay R. Amitabha De 2000 *Chem Mater* **12** 608.
[17] Song X L, Yan C Y, Huang S T, Zhang M W, Geng B Y, Meng R Bin 2013 *Advanced Materials Research* **750** 1098–1103.
[18] Zagorny M, Bykov I, Melnyk A, Lobunets T, Zhygotsky A, Pozniy A, et al 2014 *J Chem Chem Eng* **8** (2) 118.
[19] Parveen A, Roy AS 2013 *Adv Mater Lett* **4** (9) 696–701.
[20] Yang C, Dong W, Cui G, Zhao Y, Shi X, Xia X, et al 2017 *Acta* **247** 486–495.
[21] Rahman KH, Kar AK 2020 *Mater Sci Semicond Process* **105** 104745.
[22] Mostafaei A, Zolriasatein A 2012 *Prog Nat Sci Mater Int* **22**(4) 273–280.
[23] Kandiel T A, Robben L, Alkaim A, Bahnemann D 2013 *Photochem Photobiol Sci* **12** (4) 602–609.
[24] Hanawalt J D, Rinn H W, Frevel L K 1938 *Ind Eng Chem Anal Ed* **10** (9) 457–512.
[25] Selvan S T, Mani A, Athinarayanasamy K, Phani KLN, Pitchumani S 1995 *Mater Res Bull* **30**(6) 699–705.
[26] Mani A, Athinarayanasamy K, Kamaraj P, Selvan S T, Ravichandran S, Phani KLNN, et al 1995 *J Mater Sci Lett* **14** (22) 1594–1596.
[27] Basavaraja C, Pierson R, Venkataraman A, Basavaraja S 2009 *Macromol Res* **17**(8) 609–615.
[28] Buerger MJ, Azaroff LV 1958 *New York: McGraw-Hill* **238** 342.
[29] Rahman KH, Kar AK 2020 *J Environ Chem Eng* **8** (5) 104181.
[30] Dobrucka R 2017 *Iran J Pharm Res IJPR* **16**(2) 756.
[31] Asha, Goyal SL, Kumar D, Kumar S, Kishore N 2014 *Indian J Pure Appl Phys* **52** (5) 341–347.
[32] Shi L, Wang X, Lu L, Yang X, Wu X 2009 *Synth Met* **159** (23–24) 2525–2529.
[33] Kao S-Y, Lin Y-S, Chin K, Hu C-W, Leung M, Ho K-C 2014 *Sol energy Mater Sol cells* **125** 261–267.
[34] Zhang Q, Bao N, Wang X, Hu X, Miao X, Chaker M, et al 2016 *Sci Rep* **6** 38066.
[35] Seif A, Nikfarjam A, ghassem HH 2019 *Sensors Actuators B Chem* **298** 126906.
[36] Quillard S, Louarn G, Lefrant S, MacDiarmid AG 1994 *Phys Rev B*, **50** (17), 12496.
[37] Socrates G 2004 *John Wiley & Sons*.
[38] Zhang L, Liu P, Su Z 2006 *Polym Degrad Stab* **91** (9) 2213–2219.
[39] Min S, Wang F, Han Y 2007 *J Mater Sci* **42** (24) 9966–9972.
[40] Allen JE, Ray B, Khan MR, Yager KG, Alam MA, Black CT 2012 *Appl Phys Lett* **101** (6) 63105.
[41] Olad A, Behboudi S, Entezami AA 2012 *Bull Mater Sci* **35** (5) 801–809.
[42] Li X, Wang D, Luo Q, An J, Wang Y, Cheng G 2008 *J Chem Technol Biotechnol Int Res Process Environ Clean Technol* **83** (11) 1558–1564.
[43] Wang H, Han B, Lu J, Wu P, Cui W 2020 *Mater Lett* **260** 126906.
[44] Mir FA 2010 *J Optoelectron Biomed Mater* **2** (2) 79–84.
[45] Xia H, Wang Q 2002 *Chem Mater* **14** (5) 2158–2165.
[46] Su S-J, Kuramoto N 2000 *Synth Met* **114** (2) 147–153.

[47] Cionti C, Pina C Della, Meroni D, Falletta E, Ardizzone S 2020 *Nanomaterials* **10** (3) 10030441.
[48] Takpire SR, Waghuley SA 2017 *J Energy Inst* **90** (1) 44–50.
[49] Pankove JI 1975 *Courier Corporation.*
[50] Ahmadi M, Ghasemi MR, Rafsanjani HH 2011 *J Mater Sci Eng* **5** (1) 87.
[51] M. Reda S, M. Al-Ghannam S 2012 *Adv Mater Phys Chem* **02** (02) 75–81.
[52] Kulkarni M, Patil-Sen Y, Junkar I, Kulkarni C V, Lorenzetti M, Iglič A 2015 *Colloids Surfaces B Biointerfaces* **129** 47–53.
[53] Carré A 2007 *J Adhes Sci Technol* **21** (10) 961–981.
[54] Siddiqa AJ, Chaudhury K, Adhikari B 2015 *Res Rev J Med Chem* **1** 43–54.
[55] Leroy F, Müller-Plathe F 2010 *J Chem Phys* **133** (4) 44110.
[56] Psarski M, Pawlak D, Grobelny J, Celichowski G 2019 *Appl Surf Sci* **479** 489–498.
[57] Gongadze E, Velikonja A, Perutkova Š, Kramar P, Maček-Lebar A, Kralj-Iglič V, et al 2014 *Electrochim Acta* **126** 42–60.
[58] Good RJ 1992 *J Adhes Sci Technol* **6** (12) 1269–1302.
[59] Pereira VR, A M Isloor, A K Zulhairun, M N Subramaniam, W J Lau and A F Ismail 2016 *RSC Adv* **6** (102) 99764–99773.
[60] Jlassi K, Radwan AB, Sadasivuni KK, Mrlik M, Abdullah AM, Chehimi MM, et al 2018 *Sci Rep* **8** (1) 1–13.
[61] Deshpande NG, Gudage YG, Sharma R, Vyas JC, Kim JB, Lee YP 2009 *Sensors Actuators B Chem* **138** (1) 76–84.
[62] Arora R, Mandal UK, Sharma P, Srivastav A 2014 *Procedia Mater Sci* **6** 238–243.
[63] Su B, Min S, She S, Tong Y, Bai J 2007 *Front Chem China* **2** (2) 123–126.
[64] Zagorny M, Bykov I 2014 *J Chem Eng Chem Res* **1** (1) 6–14.
[65] Pud AA, Ogurtsov NA, Noskov Y V, Mikhaylov SD, Piryatinski YP, Bliznyuk VN 2019 *Semicond Physics Quantum Electron & Optoelectron* **22** (4) 470-478.
[66] Ogurtsov NA, Noskov Y V, Fatyeyeva KY, Ilyin VG, Dudarenko G V, Pud AA 2013 *J Phys Chem B* **117** (17) 5306–5314.
[67] Li X, Chen W, Bian C, He J, Xu N, Xue G 2003 *Appl Surf Sci* **217** (1–4) 16–22.
[68] Diantoro M, Suprayogi T, Taufiq A, Fuad A, Mufti N 2019 *Mater Today Proc* **17** 1197–1209.
[69] Geethalakshmi D, Muthukumarasamy N, Balasundaraprabhu R 2016 *Mater Sci Semicond Process* **51** 71–80.
[70] Nemade K, Dudhe P, Tekade P 2018 *Solid State Sci* **83** 99–106.
[71] Elumalai NK, Uddin A 2016 *Energy Environ Sci* **9** (2) 391–410.
[72] Babaei Z, Rezaei B, Pisheh MK, Afshar-Taromi F 2020 *Mater Chem Phys* **248** 122879.
[73] Ibrahim M, Bassil M, Demirci UB, Khoury T, Moussa GEH, El Tahchi M, et al 2012 *Mater Chem Phys* **133** (2–3) 1040–1049.
[74] Liu Z, Zhou J, Xue H, Shen L, Zang H, Chen W 2006 *Synth Met* **156** (9–10) 721–723.
[75] Stojanović GM, Radetić MM, Šaponjić Z V, Radoičić MB, Radovanović MR, Popović Ž V, et al 2020 *Appl Sci* **10** (12) 4392.